J. Fluid Mech. (1978), *vol.* 84, *part* 4, *pp.* 695–704
Printed in Great Britain

Visual observation of natural convective flow in a narrow vertical cavity

By NOBUHIRO SEKI, SHOICHIRO FUKUSAKO AND HIDEO INABA

Department of Mechanical Engineering, Faculty of Engineering, Hokkaido University, Sapporo 060, Japan

(Received 5 April 1977)

Experimental visualization of natural convective flow was carried out by using several kinds of fluid contained in a narrow vertical rectangular cavity with one vertical wall heated, the opposing vertical wall cooled and the upper and lower walls insulated. The effects of the Prandtl number Pr of the working fluid and the width of the cavity W on the flow pattern are discussed qualitatively in the present paper. The occurrence of flow patterns consisting of unicellular flow, steady secondary flow, tertiary flow and transition (from laminar to turbulent) flow is categorically demonstrated by the photographs taken. Moreover, experimental measurements of the net heat transfer through the vertical fluid layer are given for aspect ratios of 6–30 and Prandtl numbers of 4–12500.

1. Introduction

The earliest study of heat transfer in air in a rectangular cavity with one vertical wall uniformly heated and the opposing vertical wall uniformly cooled was performed by Nusselt (1909). Later, Eckert & Carlson (1961) measured the temperature distributions in an air layer with a Mach–Zehnder interferometer and obtained useful information on the local heat transfer on the vertical walls. However, they did not clarify the influence of the physical properties of the working fluid on heat transfer because their experiments were performed with air only. Recently, Elder (1965) measured the temperature and velocity profiles in a vertical narrow slot whose upper region was filled with air by using several kinds of fluids with a high Prandtl number Pr and observed the existence of steady multicellular flows (secondary and tertiary flows). However, he did not succeed in making correct visual observations of the flow pattern because the streaklines of tracer particles sometimes disappeared owing to a change in the direction of the light beam reflected from the disk-shaped aluminium particles used as tracer particles. Moreover, he tried to demonstrate analytically the existence of multicellular flows by superimposing a spatially periodic disturbance on an approximate model of the base flow. However, a correct comparison between the experimental streaklines and the numerical results could not be carried out because the upper boundary for his experiment was a free surface while that for his analysis was a rigid surface.

As will be evident, the effects of the Prandtl number and the width of the cavity on the flow pattern and the heat transfer through the vertical fluid layer have not been fully discussed. Therefore the present study is focused on investigating the

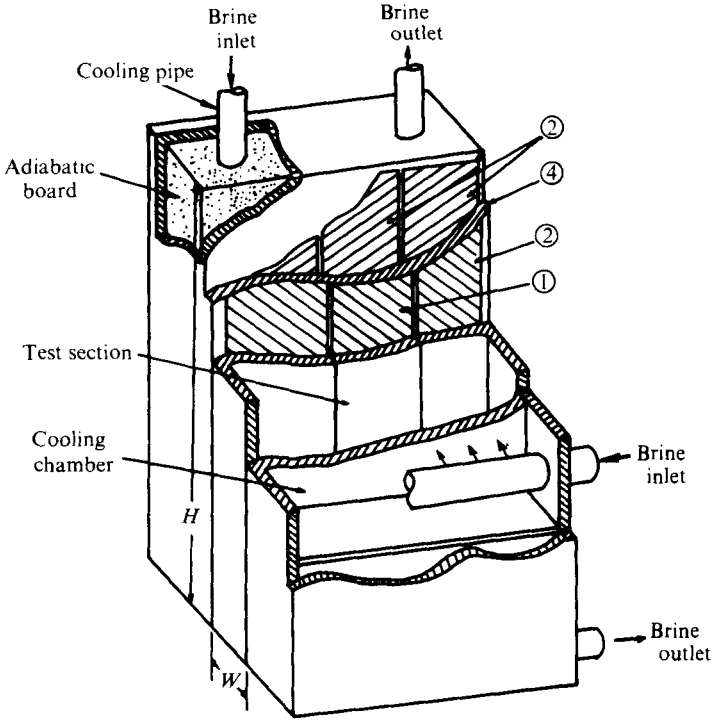

FIGURE 1(*a*). For legend see facing page.

effects of the Prandtl number and the cavity width on the flow pattern in a narrow vertical cavity having a no-slip upper boundary, one vertical wall uniformly heated, the opposing vertical wall uniformly cooled and the upper and lower walls insulated. In order to observe the flow patterns in detail, the experimental visualization was performed with polystyrene spheres as the tracer particles instead of the aluminium particles used in previous studies. Moreover, an attempt is made to compare the flow patterns obtained by visual observation with those obtained by solving numerically the partial differential equations for the conservation of mass, momentum and energy. Finally, the correlation for heat transfer through the vertical fluid layer is presented on the basis of the flow patterns.

2. Experimental apparatus and procedure

Description of the apparatus

The present experiments were carried out in a vertical rectangular cavity 300 mm high and of variable width. The experimental apparatus is depicted in figure 1. The two vertical walls (the hot and cold walls), which consist of copper plates (5 mm in thickness), are separated by narrow lucite frames of variable width (10 mm, 20 mm or 50 mm). Three independent stainless-steel foils (50 μm in thickness) are used as the main heaters for the hot wall, whose surface temperature is maintained uniform during the runs. The guard heaters mounted on the backs of the main heaters were installed to minimize the heat loss from the main heaters to the environment. The surface temperature of the cold wall is maintained uniform by using three inde-

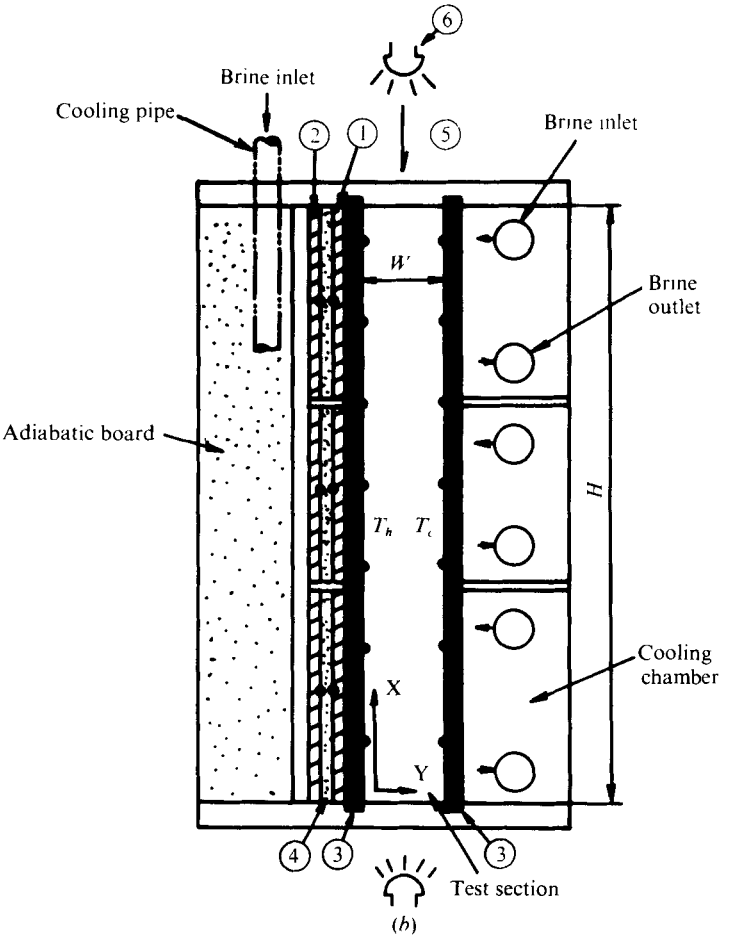

FIGURE 1. Schematic diagram of the experimental apparatus. ●, thermocouple; ①, main heater; ②, guard heater; ③, copper plate; ④, bakelite plate; ⑤, traversing thermocouple; ⑥, lamp.

pendent temperature-controlled coolants delivered into each cooling chamber attached outside the cold wall.

Thirteen copper–constantan thermocouples (0·3 mm in diameter) are soldered onto the hot and cold walls and an additional eighteen thermocouples are attached to the heaters. Their power outputs are recorded with a precision potentiometer. In all the runs, the vertical temperature gradient measured on both vertical walls was less than 0·02 °C/cm.

The experimental apparatus was covered by insulating material except during the operating period of visualization. The experimental apparatus was placed in a temperature-controlled room to prevent interference from the environment. Water (Pr = 7·1 at 20 °C), transformer oil (Pr = 480) and glycerin (Pr = 12 500) were used as the working fluids.

Visualization

For the visualization of the flow patterns, two 100 W projection lamps and two narrow slits (3 mm in thickness) were mounted on the upper and lower walls. The tracer consisted of polystyrene particles (about 0·2 mm in diameter) or detergent according to the kind of working fluid. The preferred time exposure for the photographs was between 20 and 90 s. The photographs were taken after a steady state had been reached in the test section, thermally as well as hydrodynamically. It took about 2–4 h to obtain this steady state.

Physical properties of the working fluids are evaluated at the average of the surface temperatures of the hot and cold walls. The non-dimensional numbers used in the present study are

$$Pr = \nu/k \text{ (Prandtl number)}, \quad H/W \text{ (aspect ratio)},$$

$$Nu_H = qH/\lambda\Delta T \text{ (Nusselt number)}, \quad Ra_H = g\beta\,\Delta T\,H^3/\nu k \text{ (Rayleigh number)}.$$

Here the height of the cavity is denoted by H, the width of the cavity by W, gravity by g, the heat conductivity by λ, the temperature difference between the hot and cold walls by ΔT, the kinematic viscosity by ν, the thermal expansion coefficient by β and the heat transferred per unit area by q.

3. Results and discussion

The intriguing typical flow patterns visualized are shown in figures 3–6 (plates 1–7). In each figure the hot wall is on the left and the cold wall on the right.

The primary and secondary flows

The various flow patterns produced by the temperature difference between the two vertical walls for $H/W = 15$ ($W = 20$ mm) and transformer oil are shown in figure 3 (plates 1–3) for various Ra_H. It is notable that if polystyrene spheres are used as the tracer particles one can obtain clearer streaklines than those obtained in previous studies, for example Elder's (1965) observations obtained with aluminium powder as the tracer.

Figure 3(*a*), for $Ra_H = 4{\cdot}5 \times 10^8$, which corresponds to a small temperature difference between the two vertical walls, shows a primary flow circulating from the hot wall to the cold wall (clockwise in the figure). At about $Ra_H = 6{\cdot}0 \times 10^8$, steady secondary flows with the same sense of circulation as the primary flow, whose existence was reported by Elder (1965), are observed inside the primary flow in the central core region at the mid-height of the cavity. Figure 3(*b*) shows a typical photograph of the developed secondary flow for $Ra_H = 1{\cdot}0 \times 10^9$.

Numerical verification of convection for the primary and secondary flows

The numerical analysis is carried out to predict qualitatively the existence of the flow patterns found by visual observation, and shown in figures 3(*a*) and (*b*). In the present study, the two-dimensional numerical solutions are obtained by solving a finite-difference approximation of the steady Boussinesq equations as in previous

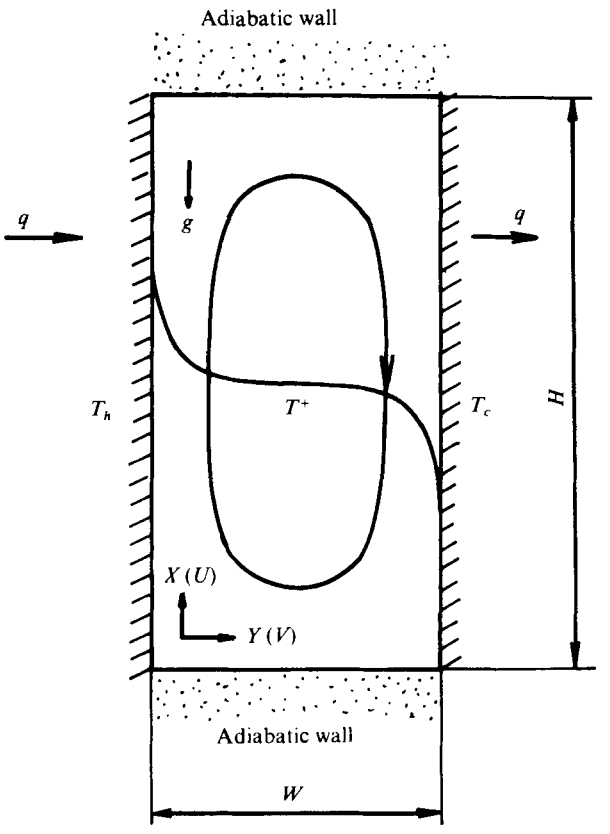

FIGURE 2. Physical model of the cavity.

investigations (e.g. de Vahl Davis & Mallinson 1975; Vest & Arpaci 1969). We attempt to improve the convergence of the present numerical solutions by introducing a length divided by viscosity and the square root of the Grashof number into the non-dimensionalizing factor for the velocity, as proposed by Plows (1968). The physical model is shown in figure 2. We introduce a stream function Ψ, the vorticity ω and the following non-dimensional variables into the equations of conservation of mass, momentum and energy:

$$X^+ = \frac{X}{W}, \quad Y^+ = \frac{Y}{W}, \quad U^+ = \frac{UW}{\nu Gr_w^{\frac{1}{2}}}, \quad V^+ = \frac{VW}{\nu Gr_w^{\frac{1}{2}}}, \quad \Psi^+ = \frac{\Psi}{\nu Gr_w^{\frac{1}{2}}},$$

$$\omega^+ = \frac{\omega W^2}{\nu Gr_w^{\frac{1}{2}}}, \quad T^+ = \frac{T-T_c}{T_h-T_c}, \quad Pr = \frac{\rho c_p \nu}{\lambda}, \quad Gr_w = \frac{g\beta(T_h-T_c)W^3}{\nu^2},$$

where ρ is the density and c_p the specific heat. This gives the following non-dimensional governing equations to be analysed:

$$\frac{\partial}{\partial X^+}\left(\frac{\partial \Psi^+}{\partial X^+}\right) + \frac{\partial}{\partial Y^+}\left(\frac{\partial \Psi^+}{\partial Y^+}\right) + \omega^+ = 0,$$

$$\frac{\partial}{\partial X^+}\left(\omega^+ \frac{\partial \Psi^+}{\partial Y^+}\right) + \frac{\partial}{\partial Y^+}\left(\omega^+ \frac{\partial \Psi^+}{\partial X^+}\right) - \frac{1}{Gr_w^{\frac{1}{2}}}\left[\frac{\partial}{\partial X^+}\left(\frac{\partial \omega^+}{\partial X^+}\right) + \frac{\partial}{\partial Y^+}\left(\frac{\partial \omega^+}{\partial Y^+}\right)\right] + \frac{\partial T^+}{\partial Y^+} = 0,$$

$$Pr\left[\frac{\partial}{\partial X^+}\left(T^+\frac{\partial \Psi^+}{\partial Y^+}\right)-\frac{\partial}{\partial Y^+}\left(T^+\frac{\partial \Psi^+}{\partial X^+}\right)\right]-\frac{1}{Gr_w^{\frac{1}{4}}}\left[\frac{\partial}{\partial X^+}\left(\frac{\partial T^+}{\partial X^+}\right)+\frac{\partial}{\partial Y^+}\left(\frac{\partial T^+}{\partial Y^+}\right)\right]=0.$$

The boundary conditions are as follows:

$$\frac{\partial \Psi^+}{\partial X^+}=\frac{\partial \Psi^+}{\partial Y^+}=\Psi^+=0,\quad \frac{\partial T^+}{\partial X^+}=0 \quad \text{on} \quad X^+=0,$$

$$\frac{\partial \Psi^+}{\partial X^+}=\frac{\partial \Psi^+}{\partial Y^+}=\Psi^+=0,\quad \frac{\partial T^+}{\partial X^+}=0 \quad \text{on} \quad X^+=H/W,$$

$$\frac{\partial \Psi^+}{\partial Y^+}=\frac{\partial \Psi^+}{\partial X^+}=\Psi^+=0,\quad T^+=1 \quad \text{on} \quad Y^+=0,$$

$$\frac{\partial \Psi^+}{\partial Y^+}=\frac{\partial \Psi^+}{\partial X^+}=\Psi^+=0,\quad T^+=0 \quad \text{on} \quad Y^+=1.$$

The numerical computation is performed by using the upwind difference method. The number of grid points in the horizontal direction Y^+ is 21, while that in the vertical direction X^+ is 151. The same Prandtl number and Grashof number as were adopted in the present experiments are used as parameters in the numerical computation. The linear iterative method is repeated until two successive iteration values of Ψ^+, ω^+ and T^+ agree to within 0·1 %.

The computed streamlines and isotherms for $H/W = 15$ are shown in figures 3(*a*) and (*b*), respectively, together with the corresponding photographs. It may be said that the existence of the primary and secondary flows observed can be predicted qualitatively by the numerical analysis.

The tertiary and transition flows

The velocity of the secondary flow gradually increases with increasing temperature difference between the two vertical walls. Also, weak steady tertiary flows having a sense of circulation opposite to that of the primary flow begin to emerge between the secondary flows. A typical photograph of the tertiary flows (anticlockwise in the figure) is shown in figure 3(*c*) (plate 3) for $Ra_H = 5{\cdot}0 \times 10^9$ and a close-up of the tertiary flow is shown in figure 3(*d*) (plate 3). This tertiary flow which emerged between the secondary flows might be considered to be caused by the shear force due to the secondary flows.

As the temperature difference is increased, the flow in the vicinity of the upper region of the hot wall becomes unsteady and turbulent. The intriguing flow pattern shown in figure 3(*e*) (plate 3) for $Ra_H = 1{\cdot}5 \times 10^{10}$ is seen to pertain to the transition region, which consists partially of an unsteady turbulent flow as observed near the upper part of the hot wall.

Effect of working fluid on flow pattern

The flow patterns for the laminar region shown in figures 3(*a*) and (*b*) are symmetrical around the mid-height ($X = 150$ mm). This may be explained by observing that the dependence of the physical properties of transformer oil on temperature is comparatively weak in the present experimental range. However, it might be thought that the flow pattern would vary with a change in the physical properties of the fluid

used. Now we attempt visual observation with glycerin and water as the working fluid instead of transformer oil.

Figures 4(*a*)–(*c*) (plate 4) show photographs of the streaklines for glycerin, whose properties are strongly dependent on temperature. The flow pattern shown in figure 4(*a*) is similar to the primary flow shown in figure 3(*a*) for transformer oil. However, secondary flow can be observed in figure 4(*b*), for $Ra_H = 3{\cdot}5 \times 10^8$, in the upper region of the central core, but does not emerge in the lower region. Such a noticeable phenomenon as the emergence of asymmetric flow around the mid-height (X = 150 mm) seems to result from the large dependence of the viscosity of glycerin on temperature, i.e. at the above-mentioned Ra_H the viscosity of glycerin in the lower region is about forty times larger than that in the upper region. As the temperature difference between the two vertical walls is increased, the secondary flows become more developed as shown in figure 4(*c*), for $Ra_H = 1{\cdot}5 \times 10^9$.

Figure 5 (plate 5) is a typical photograph for water, at $Ra_H = 6{\cdot}0 \times 10^8$. This photograph shows that the flow contains travelling disturbances due to the lower viscosity of water. The flow pattern for water, which has a lower Pr than the other two fluids (transformer oil and glycerin), appears to become turbulent.

From the results of these visual observations over a wide range of Pr, it may be said that the flow pattern is considerably dependent on Pr.

Effect of width of cavity W on flow pattern

It is likely that the nearness of the two vertical walls may influence the growth of flow oscillations in the boundary layer. To investigate the influence of the width W on the flow pattern, the present experiments were carried out with a fixed cavity height (H = 300 mm) and various widths.

The secondary flows for transformer oil are shown in figure 6(*a*) (plate 6) for $Ra_H = 9{\cdot}5 \times 10^8$ and W = 10 mm. The reader should bear in mind the fact that in this photograph the image inside the boundary layer near the hot wall reflects the image of secondary flows caused by a large change in the density of the transformer oil in the boundary layer. However, as may be seen in figure 6(*b*) (plate 6), an unsteady flow emerges inside the primary flow for W = 50 mm at the same Ra_H ($9{\cdot}5 \times 10^8$), which corresponds to the same temperature difference between the two vertical walls. This may be regarded as the onset of turbulent flow.

Figure 6(*c*) (plate 7) is a photograph for water obtained with detergent as the tracer for $Ra_H = 9{\cdot}0 \times 10^9$ and W = 10 mm. A unicellular flow is clearly evident in this photograph. On the other hand, in figure 6(*d*), which is for W = 50 mm and the same Ra_H, the visualized flow pattern shows a very complicated behaviour as the tracer particles are moved spirally by the flow fluctuations.

It can be seen from these photographs that the flow pattern is easily transformed from laminar flow to transition flow, which has turbulent flow in part of the boundary layer, as the width of the cavity is increased.

The rate of heat transfer between the two vertical walls

The net heat transfer through the vertical fluid layer might be connected with the various flow patterns mentioned above. The relationship obtained between Nu_H and Ra_H is given in figure 7 together with two experimental correlations proposed

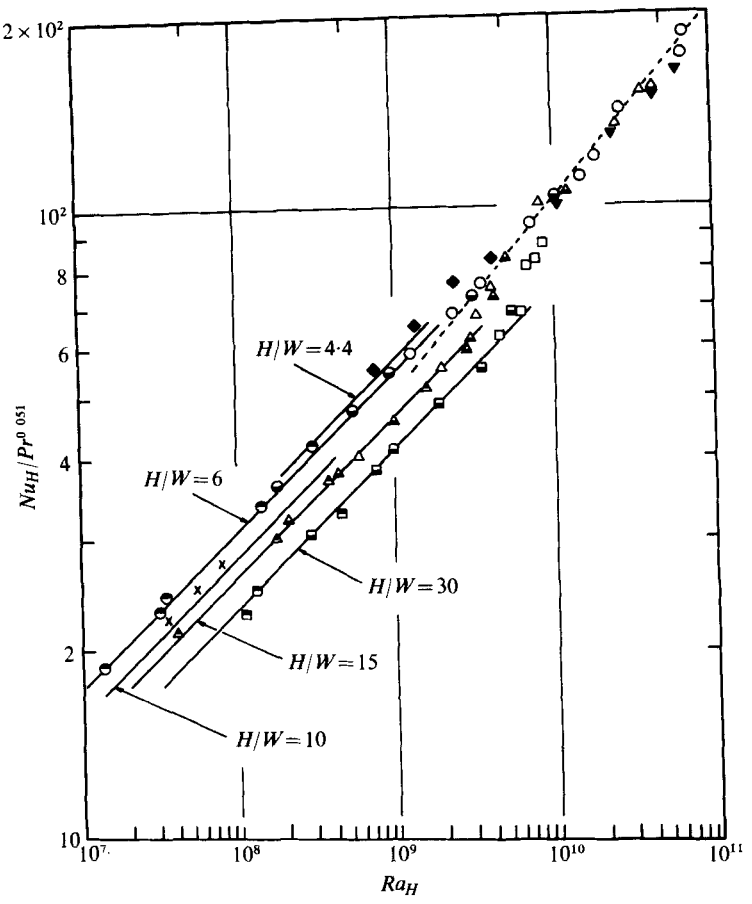

FIGURE 7. Experimental data for various convective heat transfer modes ($Nu_H/Pr^{0.051} - Ra_H$). Present experimental results: ○, water, $H/W = 6$; △, water, $H/W = 15$; □, water, $H/W = 30$; ◒, transformer oil, $H/W = 6$; ▲, transformer oil, $H/W = 15$; ⬓, transformer oil, $H/W = 30$; ◓, glycerin, $H/W = 6$; ▲, glycerin, $H/W = 15$; ⬒, glycerin, $H/W = 30$. Previous experimental results: ▼, water, $H/W = 20$, MacGregor & Emery (1969); ×, glycerin, $H/W = 10$, MacGregor & Emery (1969); ◆, water, $H/W = 4{\cdot}4$, Dropkin & Somerscales (1965). ——, present correlation for laminar region, $Nu_H = 0{\cdot}36Pr^{0.051}(H/W)^{-0.11}\,Ra_H^{0.25}$; – – –, present correlation for transition region, $Nu_H = 0{\cdot}096Pr^{0.051}\,Ra_H^{0.30}$.

by previous authors. The correlation proposed for Nu_H *vs.* Ra_H for the present study is

$$Nu_H = \begin{cases} 0{\cdot}36Pr^{0.051}(H/W)^{-0.11}\,Ra_H^{0.25} & \text{in the laminar region,} \\ 0{\cdot}096Pr^{0.051}\,Ra_H^{0.30} & \text{in the transition region,} \end{cases}$$

where the exponents of each parameter are evaluated by the root-mean-square method and its deviation is within $\pm 3\,\%$.

In figure 7, the effect of the aspect ratio H/W on heat transfer is distinguishable as $Nu_H/Pr^{0.051}$ is adopted as the ordinate. If the results in this figure are looked at from the viewpoint of the effect of the aspect ratio H/W on Nu_H, it will be seen that the mode of convective heat transfer is shifted to transition heat transfer at smaller Ra_H as H/W decreases, i.e. the shift to transition heat transfer for $H/W = 30$ occurs

at about $Ra_H = 6{\cdot}0 \times 10^9$ while that for $H/W = 4{\cdot}4$ occurs at about $Ra_H = 1{\cdot}5 \times 10^9$. This trend is verified by the above-mentioned visual observation that the flow pattern in the fluid layer is easily shifted to transition flow as the width of the cavity W increases with the height fixed, i.e. as H/W decreases.

One of our interests is to examine the effect of the secondary and tertiary flows on heat transfer. From the graph shown in figure 7, it is clear that the mode of heat transfer for the secondary flows shown in figure 3(*b*) for $Ra_H = 1{\cdot}0 \times 10^9$ and for the tertiary flows in figure 3(*c*) for $Ra_H = 5{\cdot}0 \times 10^9$ corresponds to laminar heat transfer; moreover, these flows generated by shear forces due to fluid viscosity do not contribute so much to the increase in heat transfer between the two vertical walls. On the other hand, as the flow pattern changes to transition flow as shown in figure 3(*e*) for $Ra_H = 1{\cdot}5 \times 10^{10}$, the rate of heat transfer between the two vertical walls is increased more.

In addition, we try to compare the present results with previous results. However, there is little experimental data for the present isothermal boundary conditions. Therefore we compare the present results with the results of Dropkin & Somerscales (1965) and MacGregor & Emery (1969), which were obtained under the mixed boundary conditions of an isothermal cold wall and a constant-heat-flux hot wall. The physical properties of the fluids which are needed to compare the non-dimensional parameters are evaluated at the mean of the temperatures of the hot and cold walls.

It can be seen from figure 7 that the experimental data obtained by Dropkin & Somerscales for water at $H/W = 4{\cdot}4$ and by MacGregor & Emery for glycerin at $H/W = 10$ for the laminar region lie above the solid lines proposed in the present study. These differences may be due not only to differences in the apparatus or the experimental techniques but also to the boundary conditions. However, it is very interesting that the experimental data obtained by MacGregor & Emery for water at $H/W = 20$ lie almost on the broken line proposed in the present study for the transition region. Thus, it can be said that for the transition region, in which laminar and turbulent flows coexist, the heat transfer between the two vertical walls is independent of the boundary conditions.

4. Conclusions

The variation of flow patterns with Ra_H in a rectangular cavity having one vertical wall heated and the opposing vertical wall cooled is clearly demonstrated by the visual observations. It can be seen that the flow pattern in the fluid layer is easily shifted from laminar flow to transition flow, which is partially turbulent, with decreasing Prandtl number Pr and increasing cavity width W. Moreover the behaviour of the net heat transfer between the two vertical walls is discussed on the basis of both the visual observations and a comparison between the present results and previous ones. It is clear that the mode of heat transfer for the secondary and tertiary flows corresponds to the laminar region.

REFERENCES

DROPKIN, D. & SOMERSCALES, E. 1965 *J. Heat Transfer, Trans. A.S.M.E.* **87**, 77.
ECKERT, E. R. G. & CARLSON, W. D. 1961 *Int. J. Heat Mass Transfer* **2**, 106.
ELDER, J. W. 1965 *J. Fluid Mech.* **23**, 77.
MACGREGOR, R. K. & EMERY, A. F. 1969 *J. Heat Transfer, Trans. A.S.M.E.* **91**, 391.
NUSSELT, W. 1909 *V.D.I. Forsch. Arb. Nor.* **63**, 78.
PLOWS, H. W. 1968 *Phys. Fluids* **11**, 1593.
VAHL DAVIS, G. DE & MALLINSON, G. D. 1975 *J. Fluid Mech.* **72**, 87.
VEST, C. M. & ARPACI, V. S. 1969 *J. Fluid Mech.* **36**, 1.

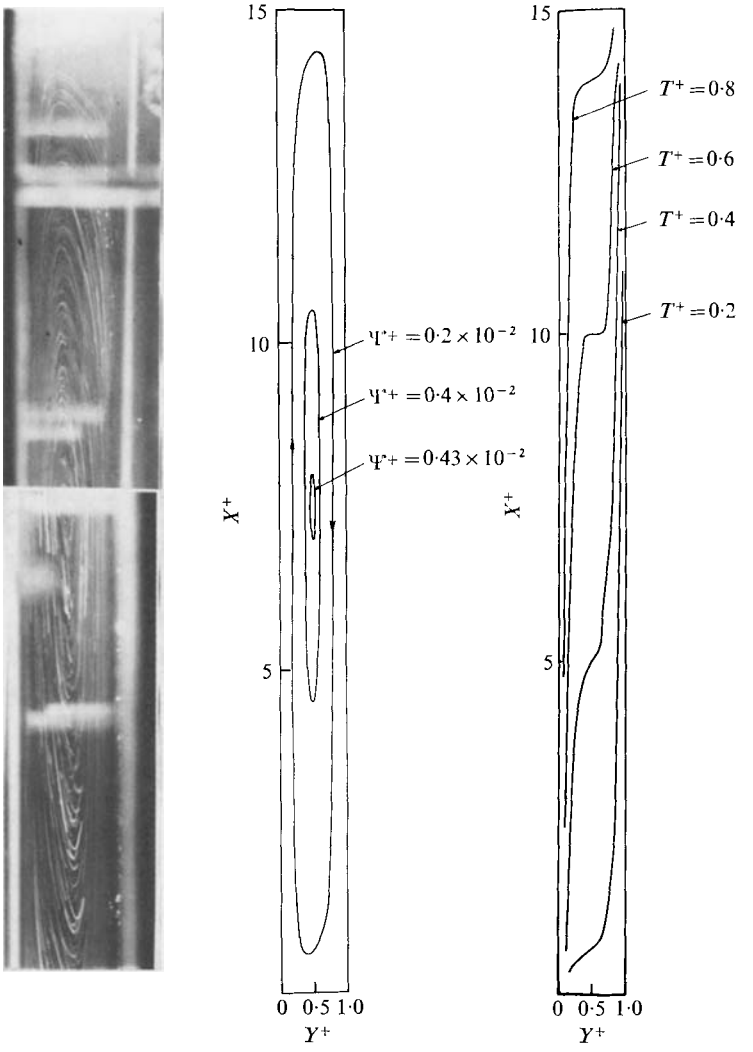

FIGURE 3(*a*). For legend see plate 3.

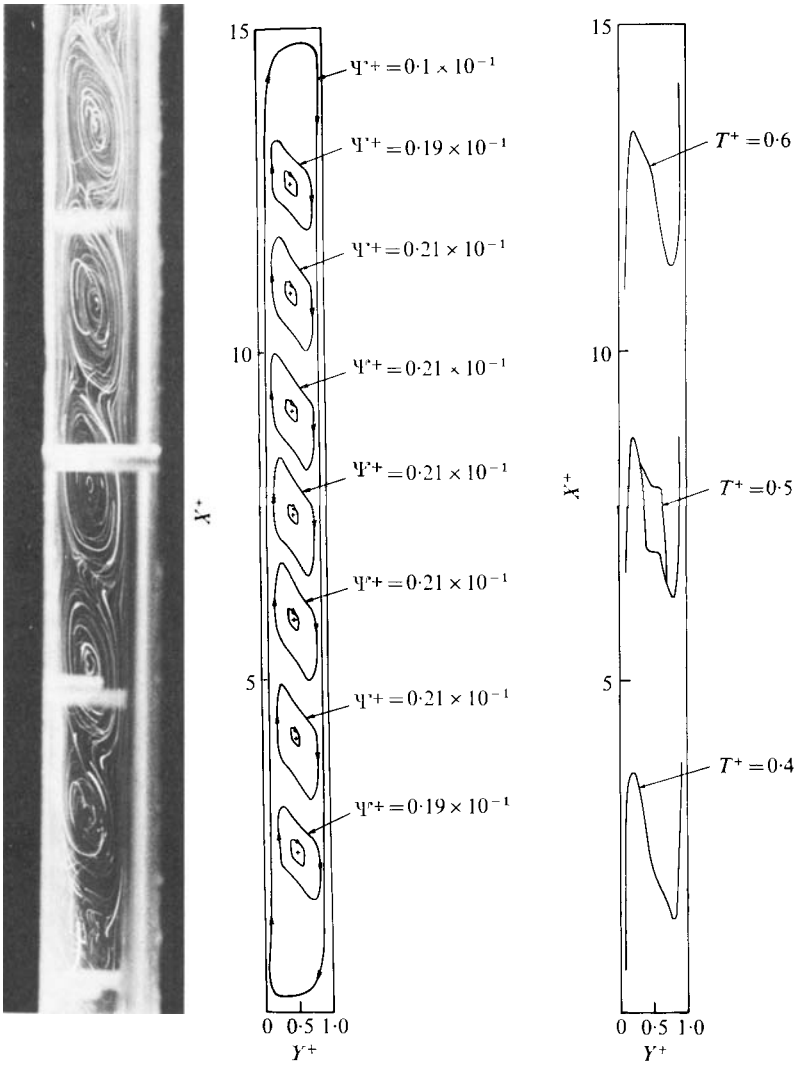

FIGURE 3(*b*). For legend see plate 3.

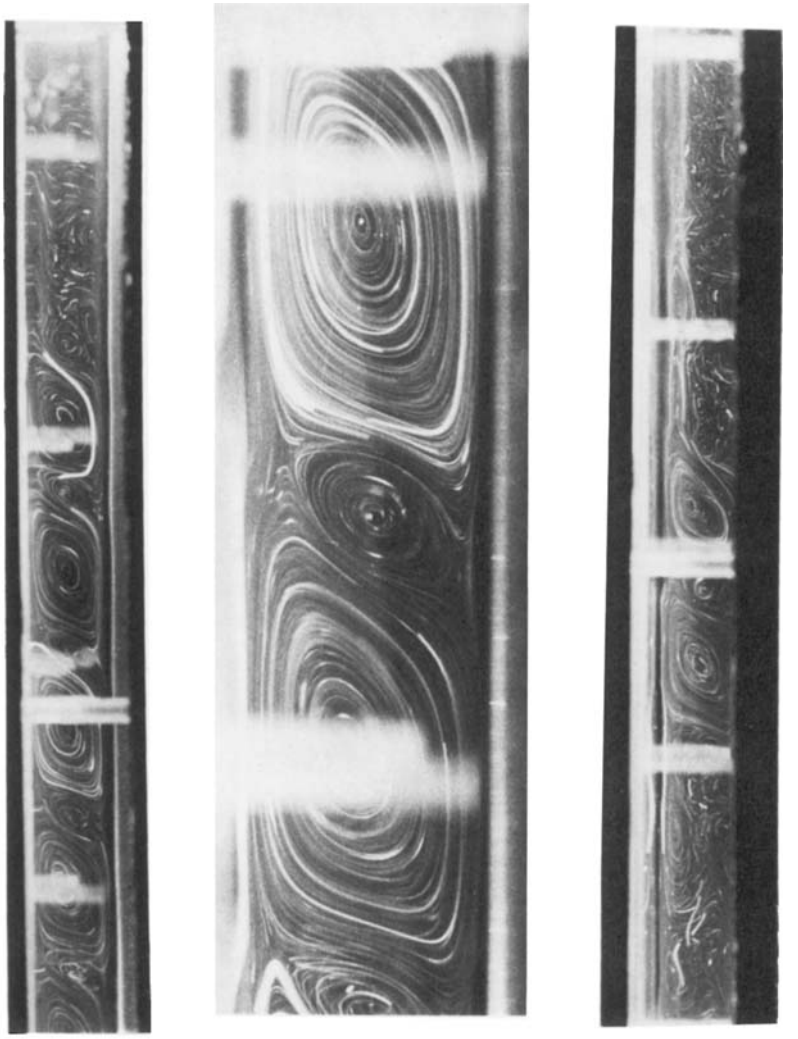

FIGURE 3. Streak photographs for transformer oil for $H/W = 15$ ($W = 20$ mm) and computed streamlines and isotherms. (*a*) $Ra_H = 4{\cdot}5 \times 10^8$. (*b*) $Ra_H = 1{\cdot}0 \times 10^9$. (*c*) $Ra_H = 5{\cdot}0 \times 10^9$. (*d*) Close-up of tertiary flow, $Ra_H = 5 \times 10^9$. (*e*) $Ra_H = 1{\cdot}5 \times 10^{10}$.

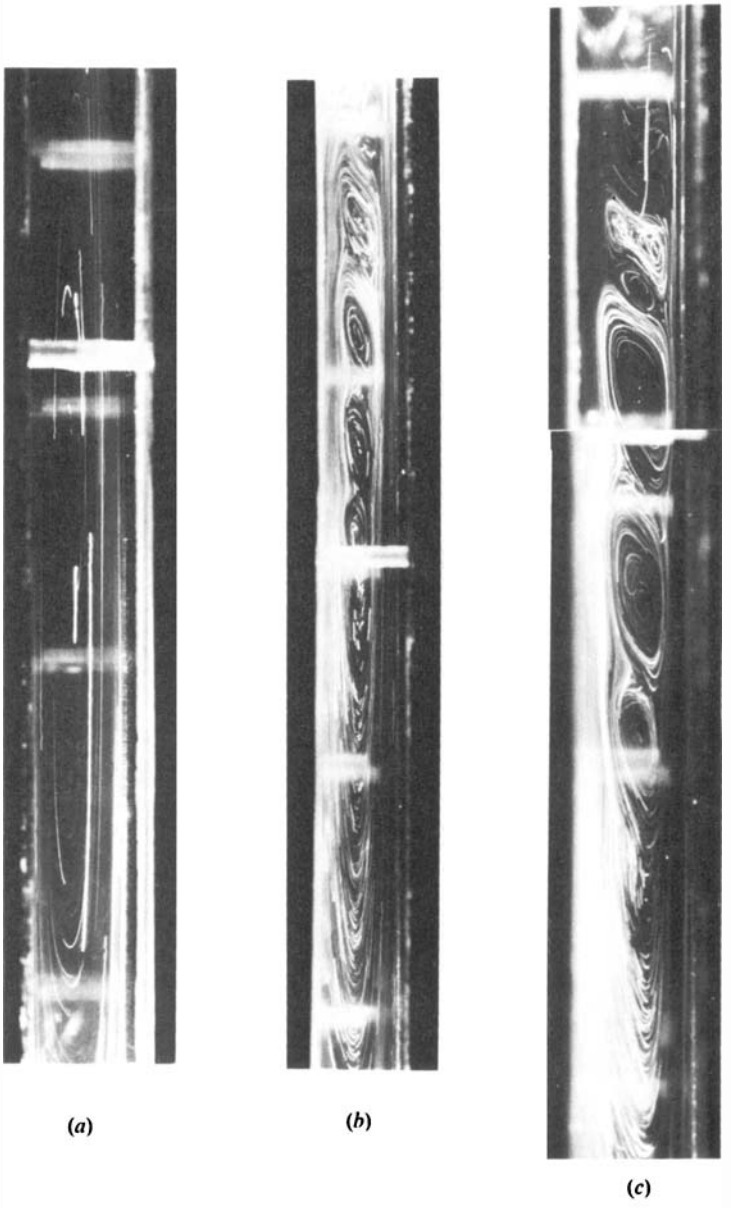

FIGURE 4. Streak photographs for glycerin for $H/W = 15$ ($W = 20$ mm). (*a*) $Ra_H = 2{\cdot}0 \times 10^8$. (*b*) $Ra_H = 3{\cdot}5 \times 10^8$. (*c*) $Ra_H = 1{\cdot}5 \times 10^9$.

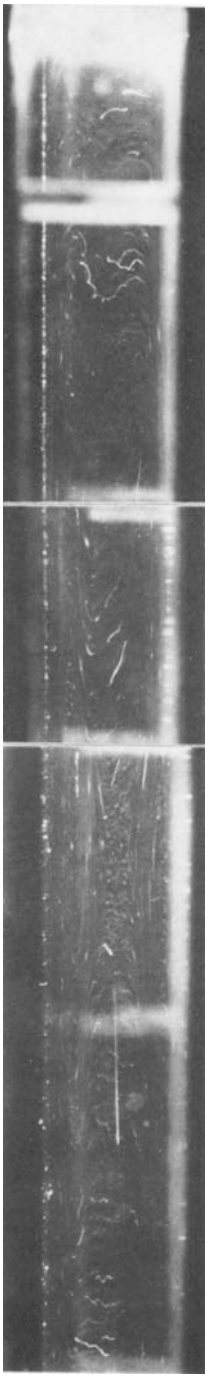

FIGURE 5. Streak photograph for water for $H/W = 15$ ($W = 20$ mm) and $Ra_H = 6{\cdot}0 \times 10^8$.

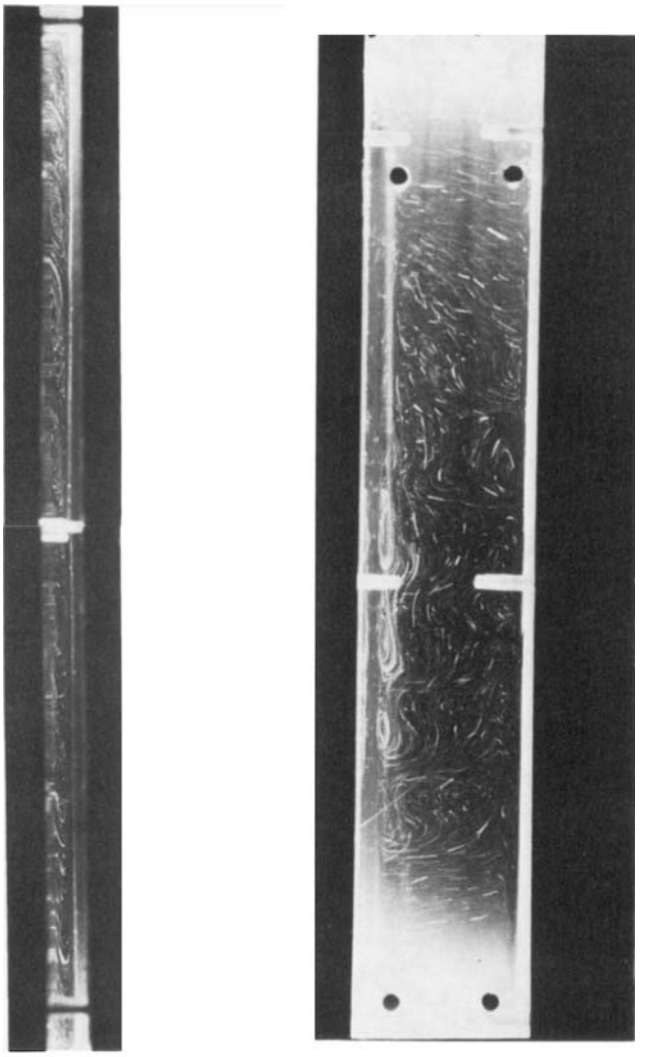

FIGURES 6(*a*, *b*). For legend see plate 7.

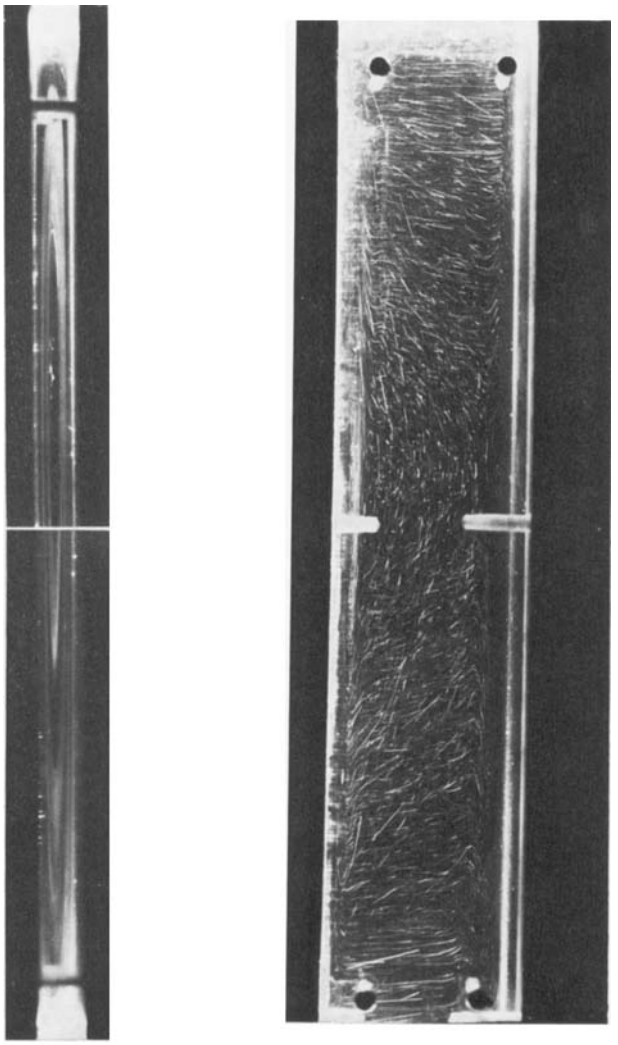

FIGURE 6. Streak photographs for transformer oil and water. (*a*) $H/W = 30$ ($W = 10$ mm), transformer oil, $Ra_H = 9{\cdot}5 \times 10^8$. (*b*) $H/W = 6$ ($W = 50$ mm), transformer oil, $Ra_H = 9{\cdot}5 \times 10^8$. (*c*) $H/W = 30$ ($W = 10$ mm), water, $Ra_H = 9{\cdot}0 \times 10^9$. (*d*) $H/W = 6$ ($W = 50$ mm), water, $Ra_H = 9{\cdot}0 \times 10^9$.